Geophysical Research Letters

RESEARCH LETTER
10.1029/2019GL085266

Eruption Interval Monitoring at Strokkur Geyser, Iceland

Eva P. S. Eibl[1], Sebastian Hainzl[2], Nele I. K. Vesely[1], Thomas R. Walter[2], Philippe Jousset[2], Gylfi Páll Hersir[3], and Torsten Dahm[1,2]

[1]Institute of Geosciences, University of Potsdam, 14476 Potsdam, Germany, [2]GFZ German Research Centre for Geosciences, Potsdam, Germany, [3]Iceland GeoSurvey (ÍSOR), 108 Reykjavik, Iceland

Key Points:
- We create a catalog of 73,466 eruptions of Strokkur geyser, Iceland, from a 1 year seismic data set
- Single to sextuple eruptions are followed by a mean waiting time of 3.7 to 16.4 min, respectively
- Waiting time after an eruption can be predicted, while future eruption type or amplitude cannot

Supporting Information:
- Figure S1
- Figure S2
- Figure S3
- Figure S4
- Figure S5

Correspondence to:
E. P. S. Eibl,
eva.eibl@uni-potsdam.de

Citation:
Eibl, E. P. S., Hainzl, S., Vesely, N. I. K., Walter, T. R., Jousset, P., Hersir, G. P. & Dahm, T. (2020). Eruption interval monitoring at Strokkur Geyser, Iceland. *Geophysical Research Letters*, *47*, e2019GL085266. https://doi.org/10.1029/2019GL085266

Received 4 SEP 2019
Accepted 2 DEC 2019
Accepted article online 10 DEC 2019

Abstract Geysers are hot springs whose frequency of water eruptions remain poorly understood. We set up a local broadband seismic network for 1 year at Strokkur geyser, Iceland, and developed an unprecedented catalog of 73,466 eruptions. We detected 50,135 single eruptions but find that the geyser is also characterized by sets of up to six eruptions in quick succession. The number of single to sextuple eruptions exponentially decreased, while the mean waiting time after an eruption linearly increased (3.7 to 16.4 min). While secondary eruptions within double to sextuple eruptions have a smaller mean seismic amplitude, the amplitude of the first eruption is comparable for all eruption types. We statistically model the eruption frequency assuming discharges proportional to the eruption multiplicity and a constant probability for subsequent events within a multituple eruption. The waiting time after an eruption is predictable but not the type or amplitude of the next one.

Plain Language Summary Geysers are springs that often erupt in hot water fountains. They erupt more often than volcanoes but are quite similar. Nevertheless, it is poorly understood how often volcanoes and also geysers erupt. We created a list of 73,466 eruption times of Strokkur geyser, Iceland, from 1 year of seismic data. The geyser erupted one to six times in quick succession. We found 50,135 single eruptions but only 1 sextuple eruption, while the mean waiting time increased from 3.7 min after single eruptions to 16.4 min after sextuple eruptions. Mean amplitudes of each eruption type were higher for single eruptions, but all first eruptions in a succession were similar in height. Assuming a constant heat inflow at depth, we can predict the waiting time after an eruption but not the type or amplitude of the next one.

1. Introduction

A geyser is a multiphase geothermal feature that exhibits frequent, jetting eruptions of hot water and non-condensable gases such as CO_2. It is composed of a conduit, a reservoir with water supply, and a heat source (Descloizeaux, 1847; Munby, 1902). No more than 1,000 such geyser systems exist worldwide (Hurwitz & Shelly, 2017).

With respect to the eruption processes, which involves bubble formation and expansion, geysers have been considered as volcano analogs (Kieffer, 1984). Geysers show a large variability in bubble-driven explosions and eruption spacing (Descloizeaux, 1847) that is similar to Strombolian-type volcanic eruptions (Taddeucci et al., 2013). At Stromboli volcano a detailed analysis suggests that single bursts, pulsations, and multiple eruptions happen (Ripepe et al., 2013). Therefore, the study of the dynamics and interdependencies of geyser eruptions may also improve the understanding of how volcanoes work (Kieffer, 1984; Hurwitz & Manga, 2017).

Geysers are small and erupt more often than volcanoes, which makes it easier to study their periodicity (Hurwitz and Shelly, 2017). For instance, the El Jefe Geyser at El Tatio, Chile, erupts as often as every 132 s (Munoz-Saez, Manga, et al., 2015). A closer examination at geysers often reveals that the waiting time between eruptions ranges from constant to irregular, bimodal or chaotic (Wang and Manga, 2010). Bimodal waiting time distributions were reported from a number of geysers worldwide, such as in El Tatio, Crystal Geyser, and Old Faithful in Yellowstone National Park (Azzalini and Bowman, 1990; Gouveia and Friedmann, 2006; Namiki et al., 2014; Munoz-Saez, Namiki, & Manga, 2015; Rinehart, 1965).

Old Faithful geyser has two modes at 50 and 70 min waiting time (Rinehart, 1965), where long eruptions predominate (3–5 min) (Hurwitz et al., 2008; Rinehart, 1980). At El Tatio, Chile, Namiki et al. (2014) reported

a mean temporal spacing of minor eruptions of 13 min 43 s and of major eruptions of 4 hr 40 min, while Gouveia and Friedmann (2006) reported waiting times of 7–32 min and 98–113 min at Crystal Geyser, USA.

The eruption frequencies of geysers are related to multiphase fluid dynamics in conduits and reservoirs (Descloizeaux, 1847). For instance, a jetting eruption occurs if the system runs into a nonlinear turning point, where accelerated flow in the conduit depressurizes the reservoir causing spontaneous degassing and a part or complete emptying of cavities in the reservoir system (e.g., Adelstein et al. (2014). Previous studies discuss different geometries and feedback processes to explain different eruption types (e.g., minor and major) and bimodal waiting time distribution after eruptions (Honda and Terada, 1906; Rinehart, 1965; Kieffer, 1984), for example, (i) boiling in the reservoir versus boiling in the conduit (Namiki et al., 2014), (ii) insufficient bubble accumulation (Gouveia and Friedmann, 2006; Munoz-Saez, Namiki, & Manga, 2015), (iii) one only partly emptied cavity (Gouveia and Friedmann, 2006; Rinehart, 1965, 1973), or (iv) multiple cavities (Hurwitz et al., 2008; Kieffer, 1984; Rinehart, 1965).

Gouveia and Friedmann (2006) suggested that at Crystal Geyser short eruptions evacuate parts of the conduit that is at that moment insufficiently charged with gas. While Rinehart (1965) speculated about two coupled cavities at Old Faithful (one from a nearby extinct geyser), Kieffer (1984) reported two storage regions and Rinehart (1973) interpreted this behavior as one reservoir that only partly empties during minor eruptions.

Geyser eruption dynamics can be influenced by changing pressure-temperature conditions. At El Tatio a major eruption occurred if bubble addition was sustained (Munoz-Saez, Namiki, & Manga, 2015) and the water in the upper conduit was heated enough (Namiki et al., 2014). Multiple minor eruptions therefore preceded a major eruption (Munoz-Saez, Namiki, & Manga, 2015). Similarly, experimental studies describe small, medium, and large eruptions and a typical sequence of multiple small eruptions before medium or large eruptions (Adelstein et al., 2014). A key requirement to quantify the variability of geyser eruptions is to install sensors collecting continuous data over long periods. Early networks consisted of a single geophone, a temperature sensor, or a video camera (Nicholls & Rinehart, 1967; Rinehart, 1968). From 1991–1994 Kedar et al. (1996) carried out an experiment using pressure sensors inside Old Faithful, six broadband seismometers, and 96 short-period vertical geophones. This data set was widely used to study the generation of geothermal tremor (Kedar et al., 1996, 1998) and the depth and location of the reservoir (Cros et al., 2011; Vandemeulebrouck et al., 2013).

The first seismic recording at Strokkur geyser in Iceland is from summer 1967, where one geophone was placed as close as possible to the boiling water pool (Rinehart, 1968). Kieffer (1984) mentions sequences of one to five eruptions in quick succession and correlates this with increasing waiting times after eruptions. These studies at Strokkur were single station approaches and did not analyze the eruptive interval in detail.

In 2017 we installed at Strokkur geyser a seismic broadband network to continuously monitor eruptions over a period of 1 year. The network was complemented for shorter periods by infrasound, tiltmeters, pressure sensors, and surveys of ground and air-based cameras (Walter et al., 2018). We identified different types of activity and created a catalog comprising 73,466 eruptions (Eibl et al., 2019). Our high-precision data set allows to study the underlying dynamics in unprecedented detail. In particular, we analyze the types and recurrence rate of multituple eruptions, their interevent times, the variations in seismic peak to peak amplitude, and energy of eruptions. We suggest a simple statistical eruption model which successfully reproduces the main characteristics of the system including multituple eruptions.

2. Data and Methods

2.1. Field Site and Experiment

The Haukadalur geothermal area in south Iceland contains over 200 geothermal anomalies, hot springs, and basins (Walter et al., 2018) including the geysers Strokkur and Great Geysir (Figure 1) (Barth, 1940; Descloizeaux, 1847). Strokkur is a pool geyser and has a silica sinter edifice with a water basin on top. The pool is about 12 m in diameter with a central tube (Rinehart, 1968) of about 2 m diameter and over 20 m depth, changing shape and temperature at 10–15 m depth (Walter et al., 2018). The geyser was penetrated by drillholes in 1963, since when it is the most active geyser in Iceland (Gudmundsson, 2017). It is filled with hot water that is constantly around its boiling point and wobbling between the eruptions until the geyser erupts (Rinehart, 1968) in a ~30 m high water column (for evolution of eruption see Walter et al., 2018).

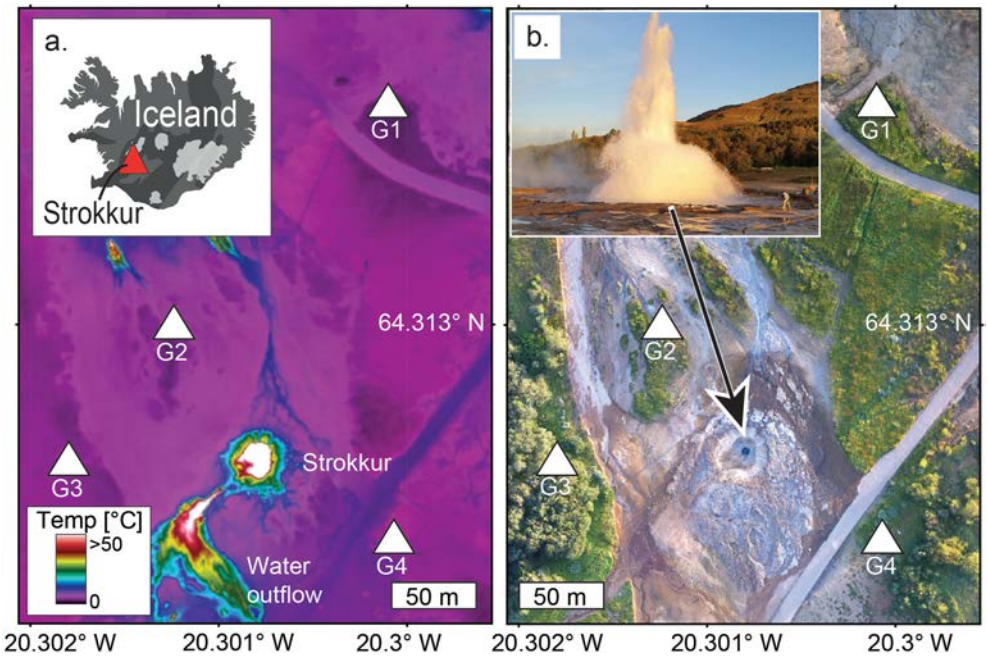

Figure 1. Map of the station network. (a) Infrared aerial image of the geothermally active region around the geyser Strokkur (after Walter et al. (2018)) showing the subaerial outflow channel to the southwest and the seismometer locations (white triangles). The inset shows the location in Iceland. (b) Aerial photo of (a). The inset shows an eruption of Strokkur in progress.

We monitored the eruptions of Strokkur geyser from 27 June 2017 to 6 June 2018 using four broadband seismic stations (Nanometrics Trillium Compact Posthole 20 s). Sensors were buried 30–40 cm deep in the ground at distances of 38.8 m (G4, SE), 47.3 m (G3, SW), 42.5 m (G2, N), and 95.5 m (G1, NE) from Strokkur center (Figure 1). Stations were regularly visited for data download or battery replacement. Data gaps represent 15.4–44.0% of the records as during the winter period maintenance intervals were longer. However, at any given time, at least one station recorded the eruptions. Despite the temporarily enhanced noise from wind, rain, and tourism, the signal-to-noise ratio (SNR) was in general sufficient to detect the geyser eruptions on all four seismometers. Station G3 was located in a small forest (Figure 1) and had the highest SNR.

2.2. Data Processing

As a first automatic processing step, the continuous data were scanned in a moving window approach. We calculated the root-mean-square of the vertical seismic data. We chose one representative eruption on 1 January 2018 at station G3 (Figure 1) and cross-correlated this eruption including its coda with the whole root-mean-square trace. Times with high correlation were saved as eruption occurrence times. The seismic fingerprint of eruptions is most likely caused by the bubble slug in the conduit, the bursting bubble, and water dropping on the ground and is characterized by most energy between 3 and 50 Hz (supporting information Figure S2).

The saved times and gaps between the saved times were then manually reviewed on highpass filtered traces with a corner frequency ~2 Hz using the pyrocko trace viewer Snuffler (Heimann et al., 2017). Wrong picks were deleted; missing picks were added. We picked the full day (24 hr) recordings from 1 December 2017 to 28 January 2018, leading to 20,390 eruption times. From 27 June to 30 November 2017 and from 29 January to 7 June 2018, 53,076 eruptions from midnight to 10 a.m. (local time, GMT + 1) were picked (Figure S1) as increased anthropogenic noise during daytime reduces the SNR.

We categorized the eruptions based on the number of eruptions in quick succession as single, double, triple, quadruple, quintuple, or sextuple eruption (Figure 2a). At Strokkur a so-called eruption coda is a typical signal indicating the end of a multituple eruption (Figure 2a). As long as the eruption coda is absent, the next eruption of the multituple set is expected "quickly."

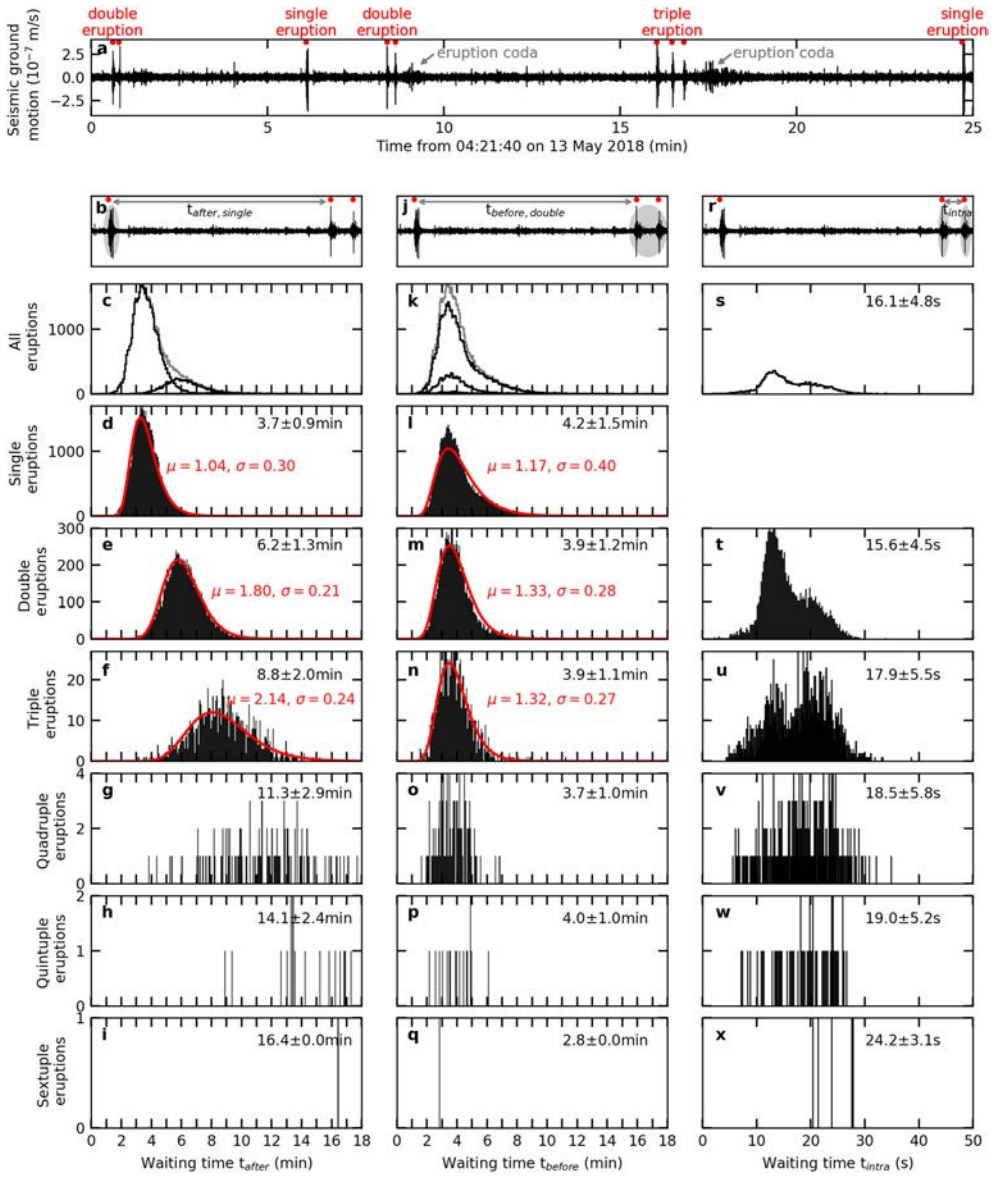

Figure 2. Recurrence time properties of different eruption types between 27 June 2017 and 7 June 2018. (a) Vertical seismic ground motion at G4 from 04:21:40 on 13 May 2018 filtered 2 to 15 Hz indicating different eruption types and eruption coda. (b–i) t_{after} for each eruption type. (c–i) Histograms with 4 s bins. Mean ± one standard deviation (black) and μ and σ values of a fitted log-normal distribution (red) are given. t_{after} for (c) all eruptions separately (black) and cumulatively (gray), (d) single eruptions, (e) double eruptions, (f) triple eruptions, (g) quadruple eruptions, (h) quintuple eruptions, and (i) sextuple eruptions. (j–q) Same as (b)–(i) but for t_{before}. (r–x) Same as (b)–(i) but for t_{intra} with 0.25 s bins.

As long as no eruption coda occurred, an event was classified as part of a multituple eruption, and the waiting time between the individual events of the set, t_{intra}, was measured. Additionally, in sequences of a multituple eruption followed by a multituple eruption we define t_{before} and t_{after} the following way: t_{before} is measured from the beginning of the first event within an eruption to the beginning of the last event of the previous eruption (Figure 2j). The time after each eruption, t_{after} (Figure 2b), was estimated from the beginning of the last event within an eruption to the beginning of the first event of the following eruption (red dots in Figures 2a and S2). The duration of the eruption or coda was not determined.

To estimate the relative strength of eruptions, we extracted an 8 s long seismogram around the eruption filtered 1 to 50 Hz starting at the time of our pick. The windowed segments were detrended, tapered, and instrument corrected to represent ground velocity. We determine the mean of the absolute minimum

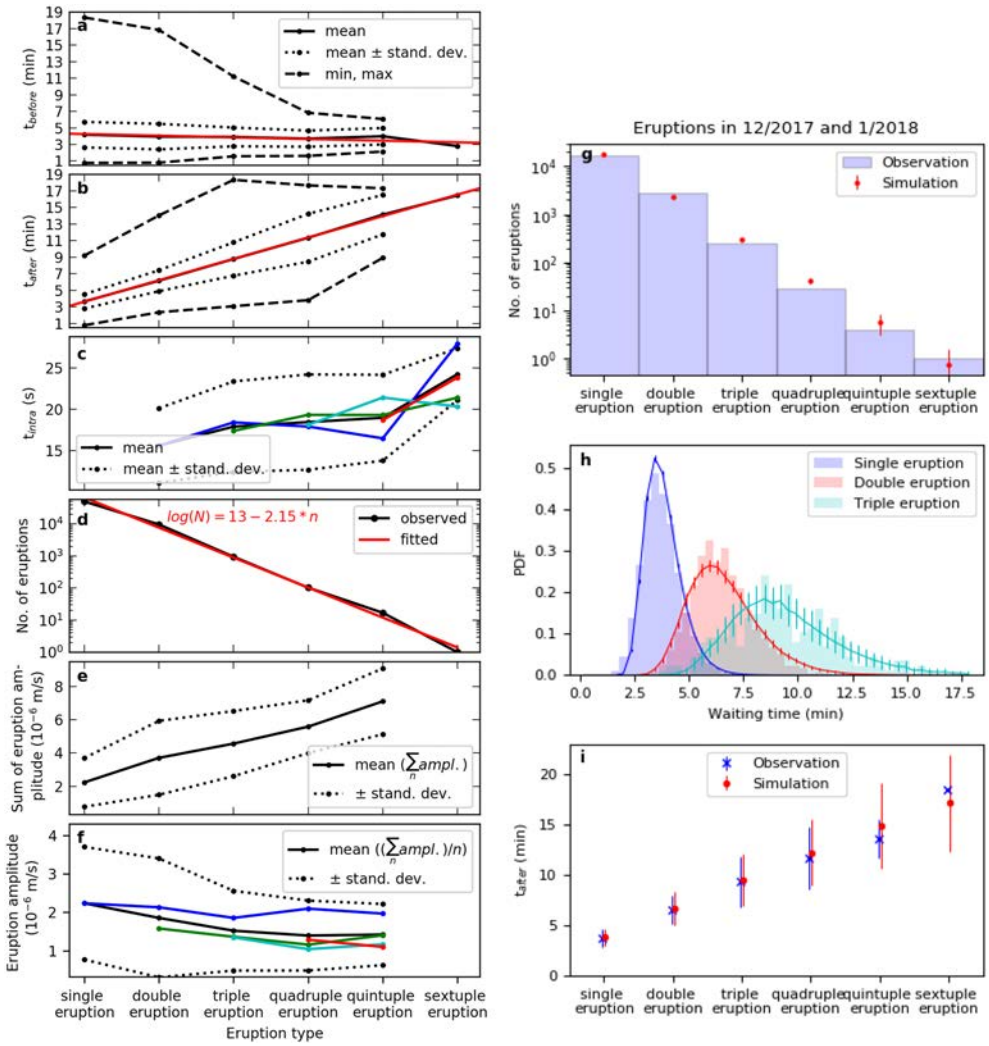

Figure 3. Mean waiting times and seismic amplitudes for each eruption type at Strokkur geyser between 27 June 2017 and 7 June 2018. (a) Mean t_{before} (solid) with one standard deviation (dotted), minimum, and maximum t_{before} (dashed). The red line refers to the result of a linear least squares regression. (b) Same as (a) but for t_{after}. (c) Mean t_{intra} within one eruption type (black) with one standard deviation (dotted). Mean t_{intra} after the first eruption (blue), second eruption (green), third eruption (cyan), and fourth eruption (red). (d) Number of single to sextuple eruptions (black) least squares fitted with $\log(N) = a - b \cdot n$ (red). Note that the y axis is logarithmic. (e) Mean of the sum of eruption amplitudes within single to sextuple eruptions at G4 (solid) and one standard deviation (dotted). (f) Mean amplitude of each eruption (solid black) with one standard deviation (dotted black). Mean amplitude of each first eruption (blue), second eruption (green), third eruption (cyan), and fourth eruption (red). (g–i) Comparison of simulations and observations: (g) the frequency distribution of the eruption types; (h) the probability density function (PDF) of t_{after} with $n = 1$, 2, and 3 eruptions, where lines refer to the model result; and (i) the mean ± one standard deviation of t_{after} for single to sextuple eruptions. The error bars in (g) and (h) refer to the standard deviation of the results for 100 different simulations, while the bars in (i) refer to the standard deviation of the distribution of t_{after}.

and maximum amplitude and energy in this time window to assess the relative eruption strength. This was performed for all four stations while G4 is shown (Figure 3e). The database of waiting times, event rates, peak amplitude, and energy is used for a characterization and interpretation in terms of a statistical model, which is described in detail in section 4.

3. Results

3.1. Waiting Time Distribution

For single to sextuple eruptions we study the preeruption and posteruption waiting times t_{before} and t_{after}, and the time between events within a multituple eruption, t_{intra} (Figure 2).

t_{after} strongly correlates with the eruption type. Single eruptions are on average followed 3.7±0.9 min later by the next eruption (Figure 2d). After double, triple, quadruple, quintuple, or sextuple eruptions, t_{after} is on average 6.2±1.3 min, 8.8±2.0 min, 11.3±2.9 min, 14.1±2.4 min, and 16.4 min, respectively (Figures 2e–2i). The distribution of t_{after} is fitted by a log-normal distribution with values provided in Figures 2d–2f and 2l–2n. The mean values and standard deviations of these distributions increase with the eruption multiplicity. A linear least squares regression of the eruption multiplicity n and mean t_{after} gives the equation: $t_{after} = 1.032 + 2.585 \cdot n\,(\text{min})$ with a standard error of the estimated gradient of 0.02. Therefore, the multiplicity of an eruption can be used to predict t_{after}. For example, a multiplicity of 3 would correspond to a mean waiting time of 8.8 ± 2.0 min.

In contrast, t_{before} is around 4 min for all eruption types (Figures 2l–2q) and can be fitted with $t_{before} = 4.451 - 0.199 \cdot n\,(\text{min})$ with a standard error of the estimated gradient of 0.08. The length of t_{before} can therefore not predict the eruption type of the next eruption since there is no strong correlation with the multiplicity n.

In double to sextuple eruptions the average t_{intra} slightly increases from 15.6 ± 4.5 s to 24.2 ± 3.1 s (Figures 2t–2x), where all values for t_{intra} were less than 46 s. However, the two t_{intra} values within one triple eruption are similar in length. This also holds for quadruple, quintuple, and sextuple eruptions (Figure 3c).

3.2. Variation in Eruption Strength and Energy

The ~1 year eruption database reveals that the number N of single to n-tuple eruptions follows an exponential distribution, $N \propto \exp(-bn)$, with 50,135 single eruptions, 9,683 double eruptions, 948 triple eruptions, 103 quadruple eruptions, 17 quintuple eruptions, and 1 sextuple eruption (Figure 2). A linear least squares regression yields $b = 2.15$. The corresponding fit to the observed histogram is shown in Figure 3d.

Peak to peak velocities (PGV) at stations G1, G2, G3, and G4 range from $1.5 \cdot 10^{-7}$ to $6.0 \cdot 10^{-5}$ m/s. The strongest PGV and largest standard deviations are recorded at G3 west of Strokkur despite being the second farthest station possibly due to heterogeneous ground properties (see Wu et al. (2017) at Old Faithful) or NNE-SSW aligned fractures in the area (Walter et al., 2018). The mean PGV are $6.6 \cdot 10^{-7} \pm 3.6 \cdot 10^{-7}$m/s, $2.7 \cdot 10^{-6} \pm 2.2 \cdot 10^{-6}$m/s, $4.4 \cdot 10^{-6} \pm 2.9 \cdot 10^{-6}$m/s, and $2.2 \cdot 10^{-6} \pm 1.5 \cdot 10^{-6}$ m/s at G1, G2, G3, and G4, respectively (for G4 see Figure S3).

The sum of PGV or peak energy (PE) of the events within a double to sextuple eruption is smallest for single eruptions and largest for sextuple eruptions (Figure 3e; PE not shown). The mean PE and PGV of the first event of each eruption type (blue line in Figure 3f) is on average larger than the amplitude of the second to fifth eruptions (green, cyan, and red lines in Figure 3f). It is noteworthy that the amplitudes of all first eruptions are similar in size independently of the eruption type. Furthermore, the waiting time before eruptions does not influence the eruption amplitude and vice versa; the eruption amplitude does not systematically affect the waiting time to the next event (Figures S3 and S4).

4. Discussion

4.1. Statistical Model

Based on the observed characteristics of the eruptions, we built a statistical model which reproduces the main features of the eruptive behavior. The model assumes a discharge (Δx) due to an eruption which is on average proportional to the number of eruptions in quick succession. After an eruption, reloading with a constant recharging rate ($\dot{x}_r$) starts after a fixed relaxation time (Δt_0). The latter represents the time for the erupted water to come back to the conduit which likely corresponds to the coda of the signal (Figure 2a). The next eruption occurs when a fixed threshold (x_c) is reached and consecutive secondary eruptions occur with a constant probability (p). In particular, the algorithm is the following: (i) The onset time of an eruption is deterministically calculated by $\Delta t_0 + (x_c - x(t))/\dot{x}_r$. (ii) A random number y is drawn from an uniform distribution between 0 and 1; if $y \leq p$, a second eruption follows in quick succession. This is repeated until $y > p$ and the eruption multiplicity n is given. (iii) The discharge due to the eruption is sampled from a log-normal distribution, that is, $\Delta x = n \exp(y)$ with y randomly selected from a normal distribution with zero mean and standard deviation σ. (iv) The state variable is reset to $x(t) = x_c - \Delta x$, and the next rupture time is determined by step (i).

We analyzed the eruption evolution resulting from our statistical model in the same way as the observed 20,390 eruptions recorded in December 2017 and January 2018 (24 hr windows). For the simulation results shown in (Figures 3g–3i), we set x_c arbitrarily to 0, while the relaxation time was fixed to $\Delta t_0 = 1$ min and

the loading rate to $\dot{x}_r = 0.37$ per minute to match the average waiting time t_{after} following single eruptions. The probability was chosen as $p = \exp(-2.02)$, with b=−2.02±0.08 according to the observed frequency distribution in this time period, and the parameter σ, which determines the width of the t_{after} distributions, was set to 0.29.

For the comparison, we run 100 simulations, each with the same number of eruptions as the observed one, and calculated the mean and standard deviations of the results. We find that this simple statistical model reproduces the main eruption characteristics of Strokkur. By construction, the model predicts no correlation between t_{before} and the eruption type similarly to the observed data. Furthermore, the statistical model fits the observed amount of each eruption type (Figure 3g) as well as the mean waiting times after eruptions (Figures 3h and 3i) and their distributions (Figure 3h). The increasing standard deviation of the waiting times with eruption multiplicity indicates that the uncertainty regarding the next eruption time becomes large after higher-order eruptions.

4.2. Eruption Predictability

Our eruption frequency and seismic amplitude estimations might be affected by increased anthropogenic noise level during daytime and missed, wrongly picked, and wrongly classified eruptions. Strokkur features aborted eruptions that can be seen in the seismic data but can be reliably distinguished from eruptions by not having an eruption coda. Based on our manual review, we are confident that only a small percentage of our 73,466 picks are wrong, and we can therefore reliably characterize the eruption behavior of Strokkur geyser.

Our results indicate that t_{before} cannot be used to predict the future eruption type or eruption amplitude. If the amplitude is larger, this also does not lead to a specific eruption type or longer waiting time (Figure S4). In addition, sequences of eruption types of Strokkur do not show a regular pattern. This is consistent with a seemingly irregular sequence of the short and long eruptions at Old Faithful (Rinehart, 1965) and simulated chaotic time series (Ingebritsen & Rojstaczer, 1996), but which are based on a much smaller data sample.

However, the distribution of single to sextuple eruptions statistically indicates that the system behaves deterministically as t_{after} scales linearly with the multiplicity of eruptions. This indicates that each eruption leads on average to a similar discharge. While the mean t_{after} increases linearly, the waiting time of each class is about log-normal distributed. The origin of this variability is not analyzed further here and might be due to the variability of internal eruption processes, which leads to variable discharges as assumed in our simplified statistical model, or the impact of variable external factors such as tides, pressure, temperature, and wind. While our analysis showed no changes in the geyser behavior during day and night, potential seasonal variations and effects of other external drivers are not yet clear and will be investigated in the future.

Kieffer (1984) mentioned as a side note in a paper about Old Faithful that Strokkur erupts in single to quintuple eruptions. t_{intra} was 10–20 s and $t_{after} = 0.5 + 2.5 \cdot n$ (min) was predicted with an accuracy of ±1 min. We can confirm the linear behavior of t_{after}, where our fit to the 73,466 eruption picks suggests the slightly modified relation $t = 1.15 + 2.51 \cdot n$ (min). One standard deviation of these waiting times is 0.9 to 2.9 min for single to quintuple eruptions, respectively. We also find that t_{intra} within one eruption type is stable, while t_{intra} of sextuple eruptions are slightly longer (24.2 ± 3.1 s) and amplitudes are slightly lower than for single eruptions ($t_{intra} = 15.6 \pm 4.5$ s). We therefore found a larger spread in t_{after} and a slightly longer and eruption type dependent t_{intra} and eruption amplitude in contrast to Kieffer (1984).

In our 1 year long data set, we found one sextuple eruption, while Kieffer (1984) only reported up to quintuple eruptions in a more limited data set. However, based on the observed exponential distribution, we may even expect higher-order eruptions to occur. Independently of the number of events in an eruption, it will be followed by another event with constant probability. Based on our statistical model, we may expect septuple eruptions to occur with an annual rate of 0.088, that is, once every 12 years.

4.3. Eruption Amplitude

Based on the surficial observations, we assume that the seismic peak is due to conduit processes. We find that the mean amplitude of each first event in an eruption is similar, independent of whether more eruptions follow in quick succession or not. This upper limit of the amplitude/energy might be because a large bubble squeezes through the conduit as a "slug flow." The size and transported energy of the bubble is therefore possibly limited by the conduit geometry (or the geometry of the feeder reservoir). Accordingly, Vega Rinconada Geyser, Chile, erupts in 1 m high eruptions (conduit ~10 cm wide, >8 m deep; Munoz-Saez, Namiki, &

Manga, 2015), Lone Star geyser erupts in 11–14 m high eruptions (conduit 20–40 cm wide; Karlstrom et al., 2013) and Old Faithful, USA, in 30–50 m high eruptions (1–2 m wide conduit; Cros et al., 2011). The latter is similar to Strokkur in geometry and height.

The first event of double to sextuple eruptions is on average also larger than the following events. This contrasts studies that found that medium or large eruptions are preceded by small eruptions and therefore an increase in eruption intensity with time (Adelstein et al., 2014; Azzalini & Bowman, 1990; Namiki et al., 2014). These regular eruption sequences before major eruptions in the field or lab (Adelstein et al., 2014; Namiki et al., 2014; Munoz-Saez, Namiki, & Manga, 2015) contrast the here found irregular eruption type sequence and random spacings between eruptions of the same type.

The only eruption type that shows a bimodal behavior in waiting time between eruptions of the same type are single eruptions (Figure S5). Due to the exponential decrease of the number of eruption types from single to sextuple eruptions, single eruptions dominate and follow each other most of the time. They are sometimes replaced by a double eruption (or higher degree) leading to this bimodal distribution (Figure S5). This is however not a regular pattern in the sequence but caused by the overwhelming number of single eruptions.

As PGV and PE show, each event within a sextuple eruption releases less energy than an event within a double eruption. But in sum more energy is released by a sextuple eruption. Based on our observations in the field, we speculate that the seismic amplitude/energy reflects the fountain height rather than discharge. Since the reservoir is recharged with colder water, the system will require more time to heat that volume of water to the boiling point if more energy was lost in a multituple eruption and if we assume a constant inflow of heat at depth.

4.4. Implication for the Geyser System

Larger repose time for increased heat loss during eruptions can be explained with the model developed by Bunsen (1847, 1851) in which a temperature instability in the conduit leads to sudden boiling and eruption. However, this model cannot explain the observed spread of single to sextuple eruptions.

In contrast to our study, Rinehart (1965), Kieffer (1984), Hurwitz et al. (2008) reported that the longer waiting time occurred more often than the shorter waiting time at Old Faithful. This behavior was interpreted in the context of multiple cavities that feed the geyser. Although the eruption type distribution by Kieffer (1984) and Rinehart (1965) contrasts our distribution, a geyser system of multiple cavities might cause the here observed double to sextuple eruptions (Rinehart, 1965). The constant probability for subsequent events with a characteristic waiting time t_{intra} would require a strongly synchronized chain-like cavity structure. However, six (or more) dependent cavities to allow sextuple eruptions are unlikely and not reported in the literature.

No triggers for double to sextuple eruptions could be identified: (i) the mean amplitude of all first eruptions in a double to sextuple eruption is not increased or decreased in comparison to single eruptions. (ii) The energy released in a 0.5 to 2 hr long time window before a multiple eruption is not significantly lower.

Our predominance of single eruptions is similar to Munoz-Saez, Namiki, and Manga (2015), Namiki et al. (2014), who report multiple minor eruptions before a large eruption at El Tatio, Chile, and Gouveia and Friedmann (2006), who found two-third short eruptions and one-third long eruptions at Crystal Geyser, USA. They suggest that a large number of small eruptions prepare the system for large eruptions, for example, by accumulating a sufficient amount of bubbles or by heating the water column sufficiently. However, we do not observe a systematic eruption sequence of single eruptions leading up to, for example, double eruptions. Instead, eruptions of the same type are spaced irregularly in time (Figure S5).

In our case the eruption type sequence is random, while double to sextuple eruptions follow a statistical distribution with constant probability. This eruption behavior is possibly caused by one main cavity system at depth that drains bubbles in pulses and is only partially emptied or insufficiently charged. A geometry is needed that allows regular bubble release and potentially breaks a big bubble into several smaller ones. Similarly to Rinehart (1965), we observed that short and long eruptions start similarly but differ in length. This might suggest that both stem from one cavity or a complex cavity system that is only partly emptied during single eruptions. They observed, however, that short eruptions rarely follow each other and that areas with hotter water was in a first short eruption not triggered yet, despite being "nearly ready." In our case however, single eruptions follow each other on a regular basis.

As Strokkur was drilled and consecutively started erupting again, the Bunsen (1847, 1851) type likely contributes as an important driving mechanism. However, our study is the first one to suggest that in addition the MacKenzie (1811) model is involved. In this model eruptions are driven by a bubble trap. Given our observations and since Adelstein et al. (2014) simulated a complex geyser behavior with a simple setup of one bubble trap, we favor a one bubble trap model over a multiple bubble trap model. To create double to sextuple eruptions, we suggest that bubble traps must exist, but physical constraints and further studies, for example, of bubble volume, bubble size, eruption height, and rising velocity are needed to constrain their location and shape or other models. Since multiple eruptions cannot be created by the Bunsen (1847) model alone, observing multiple eruptions at a geyser might help to distinguish between the Bunsen (1847) and MacKenzie (1811) models.

5. Conclusion

We observed single to sextuple eruptions at Strokkur geyser in Iceland, where sextuple eruptions are composed of six water fountains. The sequence of eruptions does not show recurring patterns in eruption types. However, eruptions follow a deterministic pattern: The probability of a subsequent event within a few seconds is constant and 11.6%, which explains that the observed number of each eruption type decreases exponentially with increasing eruption multiplicity. The waiting time after eruptions scales linearly (3.7 to 16.4 min) with the eruption multiplicity, indicating that each eruption leads on average to a similar discharge. While more energy is in sum lost by multituple eruptions, it takes longer to recharge if the heat supply is constant. We suggest that the system is fed from one cavity or a number of cavities in a row at depth that constantly release bubbles in the conduit. We cannot predict whether an eruption episode stops or continues while it is ongoing. However, we can use the eruptive style to predict the mean waiting time to the next one, knowing the last eruption type. Whether this correlation between eruption amplitude and waiting time after the eruption can be transferred to forecasting volcanic eruptions and waiting times remains to be shown. A similar time-predictable model with a marked time clustering of volcanic events in open conduit systems was however reported by Marzocchi and Zaccarelli (2006). In addition, our data set will contribute to answer burning questions such as seasonal and tidal variations in time, amplitude, or spectra.

Acknowledgments
We thank the Environment Agency of Iceland and the National Energy Authority for the research permit at the Geysir geothermal field and the rangers for guidance and support. We thank the Geophysical Instrument Pool Potsdam (GIPP) for the instrument loan. This work was funded by VOLCAPSE, a research project funded by the European Research Council under the European Union's H2020 Programme/ERC Consolidator Grant [10.13039/100010663][ERC-CoG 646858]. Seismic data of this Strokkur experiment are available through GEOFON, and the event catalog is available through GFZ Data Services (Eibl et al., 2019). We thank Magnus T. Gudmundsson, Daniel Müller, Tanja Witt, Heiko Woith, and Masoud Allahbakhshi for support in the field and Johannes-Malte Mach for eruption picking.

References

Adelstein, E., Tran, A., Saez, C. M., Shteinberg, A., & Manga, M. (2014). Geyser preplay and eruption in a laboratory model with a bubble trap. *Journal of Volcanology and Geothermal Research*, *285*, 129–135. https://doi.org/10.1016/j.jvolgeores.2014.08.005

Azzalini, A., & Bowman, A. W. (1990). A look at some geyser data from Old Faithful geyser. *Applied Statistics*, *39*(3), 357–365.

Barth, T. F. W. (1940). Geysir in Iceland. *American Journal of Science*, *238*(6), 381–407.

Bunsen, R. (1847). Über den inneren Zusammanhang der pseudovulkanischen Erscheinungen Islands. *Wöhlers und Liebigs Annalen der Chemie und Pharmacie, LXII*, *62*(1), 1–59.

Bunsen, R. (1851). Physikalische Beobachtungen über die hauptsächlisten Geisire Islands. *Progress in Annalen der Physik und Chemie*, *23*(3), 197–272.

Cros, E., Roux, P., Vandemeulebrouck, J., & Kedar, S. (2011). Locating hydrothermal acoustic sources at Old Faithful Geyser using Matched Field Processing. *Geophysical Journal International*, *187*(1), 385–393. https://doi.org/10.1111/j.1365-246X.2011.05147.x

Descloizeaux, A. (1847). LX. Physical and geological observations on the principal Geysirs of Iceland. *The London, Edinburgh, and Dublin Philosophical Magazine and Journal of Science*, *30*(203), 391–409. https://doi.org/10.1080/14786444708645417

Eibl, E. P. S., Jousset, P., Dahm, T., Walter, T. R., Hersir, G. P., & Vesely, N. I. K. (2019). *Seismic experiment at the Strokkur Geyser, Iceland, allows to derive a catalogue of over 70,000 eruptions*. *GFZ Data Services*. https://doi.org/10.5880/GFZ.2.1.2019.005

Gouveia, F. J., & Friedmann, S. J. (2006). Timing and prediction of CO2 eruptions from Crystal Geyser, UT, Technical Report, https://doi.org/10.2172/897988.

Gudmundsson, A. (2017). Geysir. In *The glorious geology of Iceland's Golden Circle* (pp. 93–103). Springer International Publishing. https://doi.org/10.1007/978-3-319-55152-4

Heimann, S., Kriegerowski, M., Isken, M., Cesca, S., Daout, S., Grigoli, F., et al. (2017). Pyrocko—An open-source seismology toolbox and library. V. 0.3, Tech. rep., https://doi.org/10.5880/GFZ.2.1.2017.001

Honda, K., & Terada, T. (1906). On the geyser in atami, Japan. *Physical Review (Series I)*, *22*(5), 300–311.

Hurwitz, S., Kumar, A., Taylor, R., & Heasler, H. (2008). Climate-induced variations of geyser periodicity in Yellowstone National Park, USA. *Geology*, *36*(6), 451–454. https://doi.org/10.1130/G24723A.1

Hurwitz, S., & Manga, M. (2017). The fascinating and complex dynamics of Geyser eruptions. *Annual Review of Earth and Planetary Sciences*, *45*(1), 31–59. https://doi.org/10.1146/annurev-earth-063016-015605

Hurwitz, S., & Shelly, D. R. (2017). Illuminating the voluminous subsurface structures of Old Faithful Geyser, Yellowstone National Park. *Geophysical Research Letters*, *44*, 10,328–10,331. https://doi.org/10.1002/2017GL075833

Ingebritsen, S. E., & Rojstaczer, S. A. (1996). Geyser periodicity and the response of geysers to deformation. *Journal of Geophysical Research*, *101*(B10), 891–821.

Karlstrom, L., Hurwitz, S., Sohn, R., Vandemeulebrouck, J., Murphy, F., Rudolph, M. L., et al. (2013). Eruptions at Lone Star Geyser, Yellowstone National Park, USA: 1 Energetics and eruption dynamics. *Journal of Geophysical Research: Solid Earth*, *118*, 4048–4062. https://doi.org/10.1002/jgrb.50251

Kedar, S., Kanamori, H., & Sturtevant, B. (1998). Bubble collapse as the source of tremor at Old Faithful Geyser. *Journal of Geophysical Research*, *103*(B10), 24,283–24,299. https://doi.org/10.1029/98JB01824

Kedar, S., Sturtevant, B., & Kanamori, H. (1996). Origin of Harmonic Tremor at Old Faithful Geyser. *Nature*, *379*, 708–711.

Kieffer, S. W. (1984). Seismicity at Old Faithful Geyser: An isolated source of geothermal noise and possible analogue of volcanic seismicity. *Journal of Volcanology and Geothermal Research*, *22*, 59–95.

MacKenzie, G. (1811). Voyage to the Island of Iceland in the Summer of 1810, Tech. rep.

Marzocchi, W., & Zaccarelli, L. (2006). A quantitative model for the time-size distribution of eruptions. *Journal of Geophysical Research*, *111*, 1–13. https://doi.org/10.1029/2005JB003709

Munby, A. (1902). A model geyser. *Nature*, *65*(247).

Munoz-Saez, C., Manga, M., Hurwitz, S., Rudolph, M. L., Namiki, A., & Wang, C. Y. (2015). Dynamics within geyser conduits, and sensitivity to environmental perturbations: Insights from a periodic geyser in the El Tatio geyser field Atacama Desert, Chile. *Journal of Volcanology and Geothermal Research*, *292*, 41–55. https://doi.org/10.1016/j.jvolgeores.2015.01.002

Munoz-Saez, C., Namiki, A., & Manga, M. (2015). Geyser eruption intervals and interactions: Examples from El Tatio Atacama, Chile. *Journal of Geophysical Research: Solid Earth*, *120*, 7490–7507. https://doi.org/10.1002/2015JB012364

Namiki, A., Muñoz-Saez, C., & Manga, M. (2014). El Cobreloa: A geyser with two distinct eruption styles. *Journal of Geophysical Research: Solid Earth*, *119*, 6229–6248. https://doi.org/10.1002/2014JB011009

Nicholls, H. R., & Rinehart, J. S. (1967). Geophysical study of geyser action in Yellowstone National Park. *Journal of Geophysical Research*, *72*(18), 4651–4663. https://doi.org/10.1029/jz072i018p04651

Rinehart, J. S. (1965). Earth tremors generated by Old Faithful Geyser. *Science*, *150*(3695), 494–496. https://doi.org/10.1126/science.150.3695.494

Rinehart, J. S. (1968). Seismic signatures of some Icelandic geysers. *Journal of Geophysical Research*, *73*(14), 4609–4614.

Rinehart, J. S. (1973). Geysers, Tech. rep.

Rinehart, J. S. (1980). *Geysers and geothermal energy*, (p. 223). New York, N.Y.: Springer-Verlag.

Ripepe, M., Donne, D. D., Harris, A., Marchetti, E., & Ulivieri, G. (2013). Dynamics of Strombolian Activity. *Geophysical Monograph Series*, 39–48. https://doi.org/10.1029/182gm05

Taddeucci, J., Palladino, D. M., Sottili, G., Bernini, D., Andronico, D., & Cristaldi, A. (2013). Linked frequency and intensity of persistent volcanic activity at Stromboli (Italy). *Geophysical Research Letters*, *40*, 3384–3388. https://doi.org/10.1002/grl.50652

Vandemeulebrouck, J., Roux, P., & Cros, E. (2013). The plumbing of Old Faithful Geyser revealed by hydrothermal tremor. *Geophysical Research Letters*, *40*, 1989–1993. https://doi.org/10.1002/grl.50422

Walter, T. R., Jousset, P., Allahbakhshi, M., Witt, T., Gudmundsson, M. T., & Hersir, P. (2018). Underwater and drone based photogrammetry reveals structural control at Geysir geothermal field in Iceland. *Journal of Volcanology and Geothermal Research*. https://doi.org/10.1016/j.jvolgeores.2018.01.010

Wang, C.-Y., & Manga, M. (2010). Earthquakes and water. In *Earthquakes and Water, Lecture Notes in Earth Sciences* (Vol. 114, pp. 117–123). Berlin Heidelberg: Springer-Verlag. https://doi.org/10.1007/978-3-642-00810-8_7

Wu, S. M., Ward, K. M., Farrell, J., Lin, F. C., Karplus, M., & Smith, R. B. (2017). Anatomy of Old Faithful from subsurface seismic imaging of the Yellowstone Upper Geyser Basin. *Geophysical Research Letters*, *44*, 10,240–10,247. https://doi.org/10.1002/2017GL075255